Eur. Phys. J. C (2026) 86:108
https://doi.org/10.1140/epjc/s10052-026-15353-4

THE EUROPEAN PHYSICAL JOURNAL C

Regular Article - Theoretical Physics

Cosmic ray simulation with PYTHIA

Leif Lönnblad[a], **Torbjörn Sjöstrand**

Division of Particle and Nuclear Physics, Department of Physics, Lund University, Lund, Sweden

Received: 16 December 2025 / Accepted: 22 January 2026

Abstract We present recent developments in PYTHIA for the modelling of hadronic cascades in a medium. Several improvements have been made in the Angantyr model for collisions with nuclei, especially in the limit of low collision energies, allowing it to be used throughout the hadronic cascades. Also the simplified nuclear model in the PYTHIACASCADE module has been updated. We find that the two models give consistent results for cosmic ray air showers initiated by both high energy protons and nuclei.

1 Introduction

High-energy cosmic rays can provide information on the most violent processes in the Universe. The flux is rapidly falling with energy, however, so vast experimental detectors are necessary to study the extreme high-energy tail of events. Examples of such detectors are Auger [1] for incident protons and nuclei, and IceCube [2] for neutrinos. The incident particle is not visible as such, but is detected by the interactions it induces in the medium. The products of the primary collision can interact in their turn, and so on, giving rise to a cascade of particle production. It contains two main components, the hadronic and the electromagnetic ones. The latter can arise as a by-product of the former, e.g. when π^0 mesons decay to photons.

In this article we will study the hadronic cascade evolution in the atmosphere. Core here is the modelling of a collision between a single incoming hadron or nucleus and an atmospheric nucleus. A number of different event generators have been developed to describe such collisions [3,4], notably DPMJET [5], EPOS [6–8], QGSJET [9,10], SIBYLL [11–13], and URQMD [14,15], each with several versions introduced over the years. In principle these codes could also be used for the modelling of minimum-bias QCD events at the LHC, but not for other LHC physics studies. Instead modelling of LHC pp collisions is dominated by the three general-purpose programs PYTHIA [16] HERWIG [17], and SHERPA [18]. The one area of some overlap at the LHC is heavy-ion collisions, AA and pA, where almost all studies are of a QCD character. Thus the cosmic-ray class of generators has also seen a fair amount of use, notably EPOS and URQMD, as has PYTHIA, the only heavy-ion-enabled general-purpose generator, with its ANGANTYR module [19].

It is unfortunate that the collider and cosmic-ray generator classes are so separate from each other, when so many of the physics challenges are common. Ideally one should strive to increase the overlap and thereby the cross-fertilization, but from the collider side there are some issues to overcome. For the simulation of cosmic ray cascades it is not sufficient to handle pp pA and AA interactions, but also those of any secondary hadron sufficiently long-lived to have time to interact before it decays or hits the ground: pions, Kaons, Lambdas, Sigmas, and so on. Such capability was only added to PYTHIA four years ago [20]. Another issue is that the tracking of an atmospheric cascade requires the rapid switching between different beams, targets and collision energies. This has not been possible within the ANGANTYR framework, so instead the PYTHIACASCADE – henceforth CASCADE for simplicity – add-on was introduced as a simpler first approximation, where such switching was possible. Notably, the full ANGANTYR geometry setup was replaced by a simple parametrization of the number of wounded nucleons. The CASCADE code does not handle incoming nuclei, but in the field a standard trick has been to replace an A nucleus beam with A independent protons and neutrons, sharing the full beam energy evenly [21,22].

In this article we present further development work, whereby ANGANTYR now has been expanded so that it can handle the variability already discussed above, with full nuclear geometry. This would make CASCADE obso-

[a] e-mail: leif.lonnblad@fysik.lu.se (corresponding author)

Published online: 04 February 2026

lete, except that the nuclear geometry shortcut still makes for faster execution. It has also been an important reference in the development and validation of the ANGANTYR extensions. One outcome is that the new ANGANTYR setup clarifies the distinction between elastic and inelastic cross sections, which in its turn paves the way for some adjustments to CASCADE.

We implement a simple atmospheric model for some standalone studies and comparisons presented in this article. The intention, however, is that PYTHIA should act as a valid hadronic-interaction plugin for the CORSIKA 8 tracking code [23], and that is also now possible [24,25]. In addition, already from its beginning CORSIKA 8 was set up with PYTHIA 8 as its preferred particle decay engine, where it helps that both codes are written in C++, unlike most cosmic-ray generators.

The new capabilities[1] also are relevant for other cascade tracking frameworks, notably the GEANT detector simulation program [26] that is used extensively e.g. at LHC. Since decades the earlier PYTHIA/JETSET [27] and FRITIOF [28,29] Fortran codes have here been employed for hadronic interactions, but ongoing work will make it possible to replace that with the new code described in this article. In the future we also see applications to hadronic cascades initiated by an incoming neutrino or photon, where it is "only" necessary to set up the primary interaction differently from the setup studied here.

The recent and new developments that has enabled PYTHIA usage for cosmic ray studies are introduced in Sect. 2. Thereafter Sect. 3 presents some toy studies, wherein the ANGANTYR and CASCADE setups are compared. Finally Sect. 4 provides a summary and outlook.

2 The new models

The PYTHIA generator consists of several physics components, to describe hard interactions, initial- and final-state parton showers, matching and merging between interactions and showers, multiparton interactions, beam remnants, colour reconnection, fragmentation into hadrons, decays of unstable such, and more. These components are described in the PYTHIA 8.3 guide [16], to which we refer. Instead only extensions specific to cosmic-ray applications are described here, first those that are generic enough to become parts of the basic PYTHIA machinery, and afterwards those specific to ANGANTYR and CASCADE, respectively.

2.1 New core capabilities

PYTHIA implements several models for pp and $p\overline{p}$ cross sections [30], with the default based on the Donnachie–Landshoff (DL) approach [31]. In it, the total cross section between two hadrons A and B is written as the combination of a pomeron and a reggeon term:

$$\sigma_{\text{tot}}^{AB} = X^{AB} s^{\epsilon} + Y^{AB} s^{-\eta} \,, \tag{1}$$

where s is the squared total CM energy, and a fit gives $\epsilon = 0.0808$ and $\eta = 0.4525$. The X factor is assumed to be the same for $\overline{A}B$ as for AB, while the Y factor is not. The DL article only considered a few cross sections, but the approach was extended by Schuler and Sjöstrand (SaS) [32,33]. Thus X and Y coefficients have existed for $\pi^{\pm}p$, $K^{\pm}p$, γp, $\gamma\gamma$, and separately for the $\rho^0/\omega/\phi/J/\psi$ vector meson components of the γ. This list has now been further expanded with a number of other hadrons incident on a p or a $\overline{p}$ [20]: K^0, η, η', $D^{+,0}$, D_s^+, $B^{+,0}$, B_s^0, B_c^+, Υ, Λ, Ξ, Ω, Λ_c, Ξ_c, Ω_c, Λ_b, Ξ_b and Ω_b. Baryons that only differ by the relative composition of u and d quarks or by their spin state are assumed equivalent, e.g. $\Lambda = \Sigma^+ = \Sigma^0 = \Sigma^-$. The list includes hadrons sufficiently long-lived to interact before they decay, some marginally so in a dilute atmosphere, but with better chance in the passage through solid matter.

Since there does not exist data for most of these cross sections, the Additive Quark Model (AQM) [34,35] is used, in which the pomeron X term is assumed to be proportional to the number of valence quarks, $X^{AB} \propto n_q^A n_q^B$, extended with a suppression for heavier quarks inversely proportional to the respective constituent quark mass

$$n_{q,\text{AQM}} = n_u + n_d + 0.6\, n_s + 0.2\, n_c + 0.07\, n_b. \tag{2}$$

The pattern of the Y factors is less trivial to extend to new unmeasured processes, but various considerations are used for educated guesses, such as scaling by the number of light u/d quarks that can be exchanged between A and B. In this spirit, neutron targets are assumed to give the same cross sections as proton ones, and we will use N to denote a generic nucleon, p or n, inside an equally generic nucleus A.

One consequence of the DL ansatz is that cross section ratios, such as $\sigma_{\text{tot}}^{\pi p}/\sigma_{\text{tot}}^{pp} \approx 2/3$, remain fixed at high energies. This is different from most other cosmic-ray generators, where it is assumed that all cross sections eventually converge, i.e. $\sigma_{\text{tot}}^{\pi p}/\sigma_{\text{tot}}^{pp} \to 1$ [24], based on the assumption of a universal saturation of the small-x gluon cloud. We do not know which is correct, if any, so it is necessary to keep an open mind.

The extensions to elastic and diffractive cross sections introduce further complications, and become too detailed to cover in full here, but the basic framework is the SaS one. The elastic slope B_{el}^{AB} here is a combination of hadron-specific fixed terms and a common s^{ϵ} pomeron exchange term, and from it the optical theorem gives the elastic cross section. The choice of an s^{ϵ} term rather than the conventional $\ln(s)$ term in

[1] The new features presented in this paper will be available in PYTHIA version 8.317 and onwards.

Regge theory, one ensures that $\sigma_{\rm el}(s)$ never exceeds $\sigma_{\rm tot}(s)$. For single and double diffraction again a modified Regge ansatz is used, which approximately preserves a diffractive mass spectrum shape like $\mathrm{d}m^2/m^2$, with a low-mass enhancement. The differential cross sections are integrated numerically, and their energy dependence parametrized to provide a quick selection of process type to generate in a collision. The inelastic nondiffractive cross section, which is the largest component, is defined by what is left after elastic and diffractive cross sections have been subtracted from the total one.

At energies close to threshold also other processes contribute, such as annihilation or the formation of an intermediate resonance. A framework for low-energy total and partial cross sections was introduced to PYTHIA in Ref. [36], and is used here. It is smoothly matched to the higher-energy behaviour described above.

Once a collision has been deemed to occur, a (mainly hadronic) final state has to be generated. Elastic scatterings are trivial, given the assumed $B_{\rm el}^{AB}$ above. For inelastic nondiffractive events a simple nonperturbative handling is used for CM energies up to 10 GeV, and thereafter the perturbative multiparton interaction (MPI) machinery gradually takes over.

In the nonperturbative handling, the interaction is assumed driven by the exchange of a gluon, of vanishing momentum but turning the colliding particles into colour octets. (This can be viewed as the $n_{\rm MPI} = 1$, $p_\perp \to 0$ limit of the MPI framework.) Considering only the valence content, a hadron thus is composed of a triplet quark, and a antitriplet antiquark or diquark for a meson or baryon respectively. Thereby two standard Lund strings are stretched out, each between the triplet of one hadron and the antitriplet of the other. These fragment independently of each other, to give the primary hadron products.

In the perturbative machinery, the MPI framework is driven by the perturbative interactions, such as $qq \to qq$, $qg \to qg$ and $gg \to gg$. To calculate their cross sections it is necessary to have access to parton distribution functions (PDFs) for all hadrons that may interact. Apart from the p/n, only little is know about the $\pi^\pm$, even less about $K^\pm$, and the rest is silence. Therefore the new SU21 family of PDF sets [20] is introduced for $p, \pi, K, \eta, \phi, D, D_s, J/\psi, B, B_s, B_c, \Upsilon, \Sigma, \Xi, \Omega, \Sigma_c, \Xi_c, \Omega_c, \Sigma_b, \Xi_b$ and Ω_b, where the first two are included for completeness but by default replaced by existing tunes in the literature. Inspiration comes from the leading-order GRS99 π^+ set [37], which is dynamically generated from the low starting scale $Q_0^2 = 0.26$ GeV^2. At this scale, the SU21 valence quarks are parametrized to be of the form $Nx^a(1-x)^b$. Heavier quarks are assumed to take a larger fraction of the hadron momentum than u or d ones (or than gluons), so as roughly to make all valence partons of a hadron have the same average velocity, if compared in terms of constituent masses.The u and d valence quark distributions are assumed equal within a set, and the same for all hadrons with a common heavier quark content, limiting the number of separate sets needed. The starting PDFs are evolved with QCDNUM [38] and the resulting grid files are stored in PYTHIA.

Apart from the new PDFs, and the need to handle mass effects for the heavy c and b quarks, the MPI machinery is the same as for pp. Specifically it is assumed that $p_{\perp 0}$, the lower regularization scale of the divergent $2 \to 2$ cross section, has the same energy dependence for all hadrons, which does not have to be the case. The $p_{\perp 0}$ choice, together with the PDFs, regulates the integrated MPI cross section. The average number of MPIs is then given by the ratio of the MPI cross section and the total nondiffractive one. This average feeds into the final-state multiplicity of a collision.

A technical complication is that, for each incoming hadron type and each collision energy, it is necessary to have an analytical overestimate of the differential cross section in a given $(x_1, x_2, p_\perp)$ phase space point, that can be used for Monte Carlo hit-and-miss selection down to the correct cross section. Also the integrated cross section above a given $p_\perp$ should be available for use in a Sudakov-style rejection factor. The required initialization may only take a few seconds, but that could easily be a factor 1000 slower than it takes to generate an event, so is not an option inside a cascade, where beam particles and energies change all the time. Instead results are tabulated for each of the 21 allowed incoming hadrons, and for each of them in a grid of energies, starting at 10 GeV and then logarithmically distributed upwards. For each new collision in a cascade, relevant numbers are found by energy interpolation in the respective hadron case. The full tables take several minutes to generate, but can be stored on an external file and be reused so long as none of the parameters affecting the MPI cross sections are changed. This allows for a significant speed-up of the cascade evolution.

In the spirit of the Ingelman–Schlein approach [39], a (single) diffractive subsystem can be viewed as a pomeron–hadron subcollision, where the pomeron is a composite hadron-like object, with a two-gluon valence-like content. Therefore Q^2-dependent PDFs can be defined, and that leads to MPIs. Once the cross section machinery has selected a diffractive mass, the MPI activity only depends on this mass and not on the full energy of the collision. Therefore a similar pretabulation strategy can be used as for nondiffractive events, over a grid in mass rather than in CM energy. All 21 hadrons have to be tabulated separately when the incoming hadron is diffractively scattered, given the difference in PDFs. Diffraction on the proton side only has to be tabulated once. For double diffraction the two systems can be handled separately, and so no further tabulation is required. Central diffraction, finally, can be viewed as a pomeron–pomeron collision, and only introduces one further case.

MPIs take out partons from the incoming hadrons, leaving behind a set of valence and sea remnant quarks that have to be hooked up with the rest of the outgoing partons into singlets, that then fragment. The handling of the beam remnants has a direct impact on hadron production in the forward region, which is crucial in the modelling of atmospheric cascades, since the production of a single hadron that takes almost all the incident energy (low inelasticity) gives a slower evolution of the cascade than one where the original energy is shared more equally between many hadrons (high inelasticity).

Indications are that, in pp collisions, the PYTHIA forward p/n energy spectrum is too soft and the forward γ/π^0 too hard, in spite of an energy sharing prescription where any diquark takes the bigger chunk of the remnant momentum. To address this issue, in Ref. [40] two main optional changes were introduced to make the baryon harder, i.e take more momentum. One is to reduce the so-called popcorn mechanism for a diquark at the endpoint of a string, which allows the diquark to disconnect so that a meson can be produced at the end of the string, with the baryon produced only in the second step. The other is to modify the Lund symmetric fragmentation for an endpoint diquark. The natural choice would be to use a modified a parameter for diquarks, but this turned out to give only small effects, so both modified a and b values were used. Recently, however, a bug was found in the handling of effects when a different a is picked for diquarks, as described in the PYTHIA 8.315 release documentation. Preliminarily it seems that this fix obviates the need to modify b, but more detailed studies are needed. For the moment being therefore we content ourselves with the pre-8.315 approach. It remains to be studied whether also the forward region of meson beams needs to be modified.

2.2 The ANGANTYR framework

ANGANTYR relies on the Good–Walker formalism for the Glauber calculation of cross sections and for generating events. In this way fluctuations in the nucleon–nucleon (NN) cross sections can be taken into account, in the spirit of Gribov's corrections to the original Glabuer formalism [41]. This means that ANGANTYR describes, not only *if* a nucleon in the projectile nucleus interacts with one in the target nucleus, but also *how* they interact. The procedure is described in detail in [19], and here we will only emphasise the main points.

The fluctuations in the nucleon wave function are parameterised in terms of an interaction radius, that also influences the overall elastic amplitude. By default, the this radius is allowed to fluctuate according to a Gamma distribution,

$$P(r) = \frac{r^{k-1}e^{-r/r_0}}{\Gamma(k)r_0^k}, \tag{3}$$

where k and R_0 are parameters, and $\Gamma(k)$ is the standard Gamma function. The elastic amplitude (which is approximated to be purely imaginary, with $T = \mathrm{Im}(A_{\mathrm{EL}})$) is then assumed to given by

$$T(b,\sigma) = T_0(\sigma)\ \Theta\left(\sqrt{\frac{\sigma}{2\pi T_0(\sigma)}} - b\right), \tag{4}$$

where $\sigma = (r_p + r_t)^2$ is the squared sum of the projectile and target nucleon radii, and

$$T_0(\sigma) = \left(1 - \exp\left(-\frac{\sigma_T}{\pi\sigma}\right)\right)^{\alpha}. \tag{5}$$

Here, σ_T and α are parameters which, together with the constants in the Gamma distribution can be fitted to reproduce semi-inclusive NN cross sections. From the Good–Walker formalism we get the following expressions for the total, non-diffractive inelastic, elastic, and diffractive excitation of the projectile, target and double diffractive excitation:

$$\begin{aligned}
d\sigma_{\mathrm{tot}}^{NN}/d^2b &= \langle 2T(b)\rangle_{p,t}\\
d\sigma_{\mathrm{ND}}^{NN}/d^2b &= \left\langle 2T(b) - T^2(b)\right\rangle_{p,t},\\
d\sigma_{\mathrm{EL}}^{NN}/d^2b &= \langle T(b)\rangle_{p,t}^2\\
d\sigma_{\mathrm{pex}}^{NN}/d^2b &= \left\langle \langle T(b)\rangle_t^2\right\rangle_p - \langle T(b)\rangle_{p,t}^2\\
d\sigma_{\mathrm{tex}}^{NN}/d^2b &= \left\langle \langle T(b)\rangle_p^2\right\rangle_t - \langle T(b)\rangle_{p,t}^2\\
d\sigma_{\mathrm{Dex}}^{NN}/d^2b &= \left\langle T^2(b)\right\rangle_{p,t} + \langle T(b)\rangle_{p,t}^2\\
&\quad - \left\langle \langle T(b)\rangle_p^2\right\rangle_t - \left\langle \langle T(b)\rangle_t^2\right\rangle_p.
\end{aligned} \tag{6}$$

Here $\langle\cdots\rangle_p$ and $\langle\cdots\rangle_t$ are averages over projectile and target radius respectively, and we note how the diffractive excitations are intimately connected to the fluctuations in the wave functions.

From the factorisation of the NN S-matrices, $S_{pt} = 1 - T_{pt}$, we can write down the corresponding nucleus–nucleus (AA) cross sections using the combined elastic amplitude

$$T^{AA}(b) = 1 - \prod_p \prod_t \left(1 - T^{NN}(b_{pt}, r_p r_t)\right), \tag{7}$$

where $\boldsymbol{b}_{pt} = \boldsymbol{b}_p + \boldsymbol{b} - \boldsymbol{b}_t$ is the relative impact parameter separation between a projectile and target nucleon, assuming an overall AA impact parameter, $\boldsymbol{b}$ and individual impact parameters, $\boldsymbol{b}_{p/t}$, relative to the respective nuclei.

It should be noted that, although ANGANTYR uses the expressions above to calculate the NN and AA semi-inclusive cross sections, the generated events are not exactly distributed in the same way. Considering the amplitude, T, always being positive and less than unity, it is tempting to use the different $d\sigma^{NN}/d^2b$ for a given b, r_p andr_t, as a probabilities for the different processes to occur, but since most of them includes squared averages, that is not generally possible. It does work for the non-diffractive interaction, however. Here we can generate an impact parameter, an r_p

and an r_t for the nucleons, and treat it as a probability for a non-diffractive scattering. Summing over all events will then correspond to an integration over impact parameter and averaging over projectile and target states and will give the correct non-diffractive cross section. But this is not possible for the other semi-inclusive cross sections. And even if we could, we note that for the "black" case of $T = 1$ the total "probability" would be 2, which is clearly nonsense.

The procedure implemented in ANGANTYR is to generate positions of each nucleon according to the so-called GLISSANDO [42,43] parametrrisation,[2] an overall impact parameter,[3] and a radius for each nucleon. In addition an auxiliary radius, $r'_{p/t}$, is sampled for each nucleon, in order to also sample the fluctuations in radius. In this way we have for each NN (and AA) collision four statistically equivalent samples, and the general idea is to "shuffle probabilities" between these to get the probability for a given process to happen a particular event.

To illustrate this we try to get the probability for a single diffractive target excitation as

$$P_{t\mathrm{EX}} = T(b, r_p, r_t)T(b, r_p, r'_t) - T(b, r_p, r_t)T(b, r'_p, r'_t), \tag{8}$$

which, when summed over many events will result in the correct cross section on the form $\langle\langle T\rangle_p^2\rangle_t - \langle\langle T\rangle_{pt}^2\rangle$ in Eq. (6). This probability can, however, become negative, which we solve by looking also at the other combinations with auxiliary states, to write the average probability

$$\begin{aligned} P_{\mathrm{tex}} = \frac{1}{4}\Big(&T(b, r_p, r_t)T(b, r'_p, r_t) - T(b, r_p, r_t)T(b, r'_p, r'_t) \\ +\ &T(b, r'_p, r_t)T(b, r_p, r_t) - T(b, r'_p, r_t)T(b, r_p, r'_t) \\ &T(b, r_p, r'_t)T(b, r'_p, r'_t) - T(b, r_p, r'_t)T(b, r'_p, r_t) \\ &T(b, r'_p, r'_t)T(b, r_p, r'_t) - T(b, r'_p, r'_t)T(b, r_p, r_t)\Big) \\ = \frac{1}{2}&\left(T(b, r_p, r_t) - T(b, r_p, r'_t)\right) \\ \times\ &\Big(T(b, r'_p, r_t) - T(b, r'_p, r'_t)\Big). \end{aligned} \tag{9}$$

This expression is always positive and less than unity as long as T is a monotonic function in r_t, which is the case in Eq. (5). We can therefor distribute this probability between the four states and make sure it is always positive.

In fact, the form of T we have chosen in Eq. (5) is separately monotonic in r_p and r_t, which allows us to do the same for the other inelastic diffractive cross sections.[4] Unfortunately, this procedure cannot be applied to give the correct elastic cross section.

After the Glauber simulation ANGANTYR has determined if and how any combination of projectile and target nucleon will interact. Special care must be taken in the case where, e.g., one projectile has interacted with more than one target nucleon. The procedure to handle this is to order all potential interactions according to their impact parameter, b_{pt}, starting with the most central NN sub-collision. If neither of the nucleons in such a NN pair has interacted before, the interaction is labelled primary, and a corresponding sub-event is generated by the standard machinery in PYTHIA. If both have interacted, the sub-collision is simply ignored, while if only one has interacted, the interaction is labelled secondary and treated as a diffractive excitation of the other nucleon, according to a procedure described in detail in [19] and further refined in [44].

By default, the current PYTHIA/ANGANTYR version tries to fill in as much elastic NN scatterings as possible, but it will not give the correct weight. This is a cause of some confusion for some users, as the `Pythia::stat()` function, in the case of nuclear collisions, will print out both the cross sections corresponding to the generated events, and the cross section obtained from the Glauber calculation, which do not match each other. This is expected for the elastic cross section, but is also true for the other ones. This is because the generated cross sections are listed according to the type of the *primary* NN collision, while the Glauber calculation gives the cross section for the according to the type of the full AA collision. As an example of this, consider an AA collision with only one NN single diffractive target excitation scattering, which is then also the primary interaction, and the event will be included as such in the generated cross section in the listing. In the Glauber calculation for the overall AA cross sections, however, such an event will be counted as a double diffraction event, as the elastically scattered projectile nucleon will cause that nucleus to break up as well.

To enable the generation of hadronic cascades using ANGANTYR, several developments has been made. First of all we have introduced the possibility of changing both the beam particles and the collision energy during a run. Normally ANGANTYR needs a rather lengthy initialisation procedure, involving refitting of the nucleon fluctuations to the relevant beams and energies, but now we have introduced a caching where the initialisation of a wide range of energies and beams,can be done once and for all and save to disk, to be read in future runs.

[2] The GLISSANDO parameterisation used is formally only valid for $A > 16$, but ANGANTYR uses it also for lighter nuclei by default. Options for lighter nuclei are available.

[3] By default ANGANTYR samples the whole impact parameter space using a Gaussian weighting, giving rise to weighted events, but an option to only sample within a limited region giving unweighted events is available

[4] In the current version of PYTHIA this procedure only gave the correct "wounded" cross sections, i.e., the sum of ND, DD and pEX or tEX ones, but here we will use a better strategy where all inelastic cross sections come out right.

The procedure described so far is only suitable for high collision energies. For energies below $\sim$ 20 GeV the fit to the semi-inclusive cross sections becomes very poor, and the whole fitting procedure becomes unstable. For lower energies ANGANTYR will instead use a simplified Glauber model, where the kind of sub-collision is determined only from the impact parameter, b_{pt}, Basically, if $\pi b_{pt}^2 < \sigma_{\mathrm{ND}}^{NN}$ the sub-collision is assumed to be non-diffractive, otherwise if $\pi b_{pt}^2 < \sigma_{\mathrm{ND}}^{NN} + \sigma_{\mathrm{DEX}}^{NN}$ we get a doubly diffractive excitation, and so on. In this way we also include the additional possible interactions in PYTHIA's low energy interaction machinery. This is a very naive model, which we hope to improve on in the future.

For this paper we have also introduced an alternative procedure in ANGANTYR to be used for hadronic cascades.[5] In this mode, the total generated cross section should be very close the total inelastic AA cross section. Using the unweighted impact parameter sampling it is then possible get an overestimated cross section (simply given by the sampling area). This can then be used to randomly generate the position of the next hadron collision in a medium. When calling `Pythia::next()`, ANGANTYR will now only generate one impact parameter point together with the radii and positions of all nucleons, and return `false` if no collision was produced. The user should then generate a new collision point, taking the previous failed one as starting point, and try again, and so on. The advantage of this is that there is no need for parameterising all cross sections for all types of hadrons and nuclei, these are instead obtained *on-the-fly* through the Glauber procedure.

For the results presented in this paper have chosen to not include elastic NN scatterings at all in the generation. This means that when we discuss the total inelastic AA cross section, we are referring to the part of the total cross section that involves inelastic NN scatterings. This is a reasonable approximation since the momentum of an elastically scattered incident hadron is only slightly changed and the slightly excited target nuclei is typically not observable. Hence the effect on the overall hadronic cascade should be very small.

For incident cosmic nuclei, such elastic scatterings may cause a nucleus to break up and initiate separate cascades, so there may be visible effects in this case. The modelling of nucleus remnants in ANGANTYR is, however, very crude in general, and the effect of omitting these elastic scatterings is expected to be small compared to the large uncertainties in the remnant modelling.

2.3 The CASCADE framework

Given the ANGANTYR limitations at the time, CASCADE was intended as a simpler, more flexible alternative, where the machinery for hadron–nucleon (hN) collisions of Sect. 2.1 is extended to apply to hadron–nucleus (hA) ones. It is also structured to rapidly provide the cross sections relevant for a mixed medium, such as air or ice, and on demand to perform either a collision or a decay.

Following recent modifications to ANGANTYR, and clarifications as to how its event classification works, the original CASCADE behaviour has been updated for this article. We will begin this section with an overview of the original CASCADE, and afterwards summarize those new updates.

In ANGANTYR the selection of nuclear geometry, i.e. the location of the individual nucleons in a nucleus and the incoming hadron impact parameter, takes a fair amount of time. The key information that comes out of this modelling is the number of wounded nucleons, i.e. the number of nucleons in the target that undergo a subcollision with the hadron. This probability distribution turns out to be approximately a geometrical series, and so is characterized uniquely by its average number $\langle n_{\mathrm{wound}} \rangle$. For a given nucleus A this average depends on which incoming hadron type hits with what energy, but only through the total $hN (= hp)$ cross section, as a measure of the size of the interaction region spanned by the hadron in its passage through the nucleus. The average grows approximately linearly with the hN cross section, with some corrections at small cross sections, so it is easily parametrized. Currently this has been done for fifteen common nuclei, from deuterium to lead, with interpolation for intermediate ones.

The hA cross section is now chosen to be

$$\sigma_{\mathrm{tot}}^{hA} = \sigma_{\mathrm{tot}}^{hN} \frac{A}{\langle n_{\mathrm{wound}} \rangle}, \tag{10}$$

so that the cross section for an individual nucleon to be hit is the same whether it is bound inside a nucleus or free-floating.

Thus the geometry handling is reduced to a simple scheme, starting out from a target with $n_p = Z$ protons and $n_n = A - Z$ neutrons:

1. find the hN total cross section;
2. turn this into $\langle n_{\mathrm{wound}} \rangle$, which gives the geometric series ratio $r = 1 - 1/\langle n_{\mathrm{wound}} \rangle$;
3. wound a proton or a neutron in proportions $n_p : n_n$;
4. generate the relevant subcollision, and update n_p and n_n;
5. break out of the loop with probability $1 - r$, or if there are no nucleons left;
6. else loop to 3.

The fate of the unwounded target nucleons is not addressed in this scheme. Some of them may form a new nucleus, while others break free. In the fixed-target context, however, all will have small momenta, and almost always stop before they reach the ground.

[5] Available in the setting `Angantyr:cascadeMode = on`.

Besides the geometry handling, also the event shape needs to be simulated. Each hN collision here contributes to the particle production. But each collision can take less of the incoming hadron momentum the more collisions there are. This should be reflected in a softening of the outgoing momentum spectrum for an increasing n_{wound}, and a less-than-linear increase of the total multiplicity. In the ANGANTYR model each collision leads to stretched-out Lund strings from the wounded nucleon towards the incoming hadron, e.g. as considered along a rapidity axis. Only one collision gives strings stretched all the way to the hadron, however, while the remaining have a topology more similar to a diffractive system, where the strings end in a flavour-less pomeron-like object that can be seen as having been emitted by the incoming hadron.

The details are more complicated, and again a simpler solution was created for CASCADE, with the intent to reproduce the overall pattern of ANGANTYR final-state distributions. In it, the first collision (in order of handling, with no collision time order implied) is generated as a normal hN one. The final-state particle with the highest momentum (in the direction of the incoming hadron) is then made projectile for the next subcollision, and so on. The choice of flipping the projectile identity should be viewed as a technical trick to ensure flavour conservation, not as a physical change of propagating particle. Specifically, high-energy particles are produced only after the whole hA collision. A simple rule of thumb is that particles with a momentum p are produced a distance κp away from the collision vertex, with the string tension $\kappa \approx 1$ GeV/fm. Therefore the identity flip does not affect the original hN cross section, as reflected in the n_{wound} distribution. For technical reasons, however, the handling of MPI activity in an hN collision is based on the current h particle rather than on the original one. Since e.g. πp and pp give slightly different multiplicities this is not fully consistent, but the $\pi \leftrightarrow K \leftrightarrow p$ flipping inside an hA collision reflects a similar flavour composition evolution going on in the whole atmospheric cascade, so already small differences are further diluted.

Remains to discuss the nature of each subcollision. Based on the contemporaneous understanding of ANGANTYR cross sections, the first collisions is assumed to be of any type, elastic or inelastic, while any subsequent ones are always inelastic. More specifically, a nondiffractive event is assumed to occur with probability 0.7, with the remaining corresponding to single diffraction of the target nucleon. This then roughly reproduces the ANGANTYR charged multiplicity distribution and the $\mathrm{d}n_{\text{charged}}/\mathrm{d}y$ shape. For low collision energies, where ANGANTYR does not offer any guidance, the standard PYTHIA mix of subprocesses is used.

Since the 2021 introduction of the CASCADE code, and notably in the last year, the generation and presentation of ANGANTYR cross sections has evolved, as described above. One point of confusion has been that the total cross section includes both incoherent and coherent elastic scattering, i.e. where the nucleus does or does not break up. The latter does not obey Eq. (10), but comes in addition. Furthermore, ANGANTYR cannot cleanly separate the two contributions, and so only generates inelastic collisions. By contrast, CASCADE was originally set up to generate the whole incoherent cross section, including a first elastic scattering, but any subsequent interactions was only inelastic to agree with ANGANTYR in this respect. Therefore ANGANTYR has given a higher σ_{tot}^{hA} than CASCADE, but a lower $\sigma_{\text{inel}}^{hA}$. Now elastic scatterings are removed altogether from CASCADE, either as first or as subsequent scattering. Thus Eq. (10) comes to be a statement about σ_{inel} rather than σ_{tot}, and n_{wound} only counts inelastically wounded nucleons:

$$\sigma_{\text{inel}}^{hA} = \sigma_{\text{inel}}^{hN} \frac{A}{\langle n_{\text{wound}}^{\text{inel}} \rangle}. \tag{11}$$

No longer having access to σ_{tot}^{hA} is not a limitation in the atmospheric cascade community, where $\sigma_{\text{inel}}^{hA}$ traditionally is used to compare generators. ANGANTYR bug fixes in the handling and bookkeeping of collisions has also led to increased $\langle n_{\text{wound}} \rangle$ by the order of $\sim 10\%$, and new parametrizations of the $\langle n_{\text{wound}} \rangle(\sigma_{\text{inel}}^{hA})$ have been made accordingly.

Also the nature of secondary collisions has been revisited. The removal of elastic scatterings and other changes in cross section calculations, the above-mentioned increase of $\langle n_{\text{wound}} \rangle$, and other minor changes, contribute to make the previous subprocess mix obsolete. Furthermore, a richer set of diffractive and nondiffractive topologies are allowed in ANGANTYR than assumed in the past (or well documented), which also should be taken into account. Therefore a new mix is introduced for the secondary collisions, where a fraction e_{SD} is modelled as target-side diffraction, while the rest is given as the standard composition of all inelastic collision types, including a further small fraction of target-side diffraction. A value of $e_{\text{SD}} = 0.5$ gives fair agreement between CASCADE and ANGANTYR, as seen in Fig. 1, and is used as default. Nevertheless it is a number not carved in stone, but rather offers a key parameter that easily can be varied to explore uncertainties in the atmospheric cascade evolution. Furthermore, even if the inclusive $\mathrm{d}n_{\text{chg}}/\mathrm{d}y$ distribution agrees well, this does not mean that more differential distributions fare as well. As one example, the charged multiplicity distribution is somewhat broader in CASCADE.

As a final technical note, two PYTHIA instances are used inside CASCADE. The main one performs a single hN collision, including decays of so short-lived particles that they would not have time to interact with the medium. The other is used to combine this output into an event record for the whole hA collision, or for a decay. While taken to be stable in

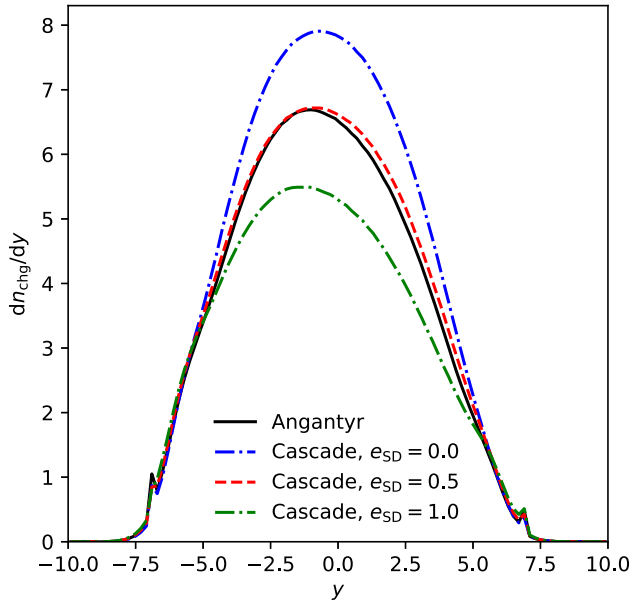

Fig. 1 Charged-particle rapidity distribution in p^{14}N collisions at 1 TeV proton–nucleon energy, comparing three values of the $e_{\rm SD}$ parameter introduced in the text

collider physics, the $\mu^{\pm}$, $\pi^{\pm}$, $K^{\pm}$ and $K^0_{\rm L}$ are here considered unstable.

3 Atmospheric cascade studies

The intention is to develop and provide models that can be used for detailed studies in a realistic context. Here we will do some simpler first studies to highlight key features of the new ANGANTYR code, and contrast them with the CASCADE code, which also has been updated. The main themes of this section is to compare basic event properties at a fixed energy or for the whole cascade evolution, and to compare incident proton and iron either for the same total energy or for the same energy per nucleon.

3.1 Cross sections

Key to the evolution of an atmospheric cascade is the hA inelastic cross section. This definition is not unique, as already mentioned. Specifically, ANGANTYR splits elastic events into true elastic and quasi-elastic, depending on whether the nucleus remains intact or split up, while CASCADE does not keep track of whether a hadron-nucleon elastic collision kicks the nucleon out of the nucleus or not. What comes out is that the Glauber formalism in ANGANTYR gives a larger elastic cross section than the simpler handling in CASCADE, and thereby a larger total one, which has led to some confusion.

In the following we will only consider the inelastic cross section. Here CASCADE and ANGANTYR have the same input hN cross section, but that does not guarantee the same subdivision of it. Leaving that aside for now, the key observable is the number of subcollisions or, equivalently, the number $n_{\rm wound}$ of (inelastically) wounded target nucleons in an hN collision. In Fig. 2a the ANGANTYR $n_{\rm wound}$ distribution is shown at a few (per-nucleon) collision energies for p^{14}N. This is the starting point for the simplified approach in CASCADE, where the results of the full nuclear geometry simulations are by a simple geometric series with the same $\langle n_{\rm wound}\rangle$, Fig. 2b. While agreement is not perfect, it is unlikely that the approximation leads to any detectable differences.

The switching between beams and energies in the atmospheric cascade evolution requires a convenient parametrization of expected $\langle n_{\rm wound}\rangle$. To a good first approximation the beams and energies should not enter individually, but only via the relevant $\sigma_{{\rm inel},hN}$ value of the two. To this end, p, π^+, K^0, ϕ^0, Σ^0, Ξ^- and Ω^- are chosen to represent meson and baryon beams of varying strangeness content, at hN CM frame collision energies $10^{(4+i)/3}$, i between 0 and 11, or energies between 21.5 GeV and 10^5 GeV. The normal ANGANTYR handling of nuclear geometry is only intended to work above 20 GeV, hence the starting scale. This gives $7 \times 12 = 84$ $\langle n_{\rm wound}\rangle(\sigma_{\rm inel})$ values, Fig. 2c, to be fitted to an interpolating formula. Inspired by the data, linear least-squares fits are made to the low- and high-$\sigma_{\rm inel}$ values separately, where the former goes up to 30 mb and the latter starts at 25 mb. The former is also constrained by $\langle n_{\rm wound}\rangle \to 1$ for $\sigma_{\rm inel} \to 0$. Henceforth $\langle n_{\rm wound}\rangle(\sigma_{\rm inel})$ is chosen as the smaller value of the two linear fits.

In Fig. 2d Eq. (11) is tested by comparing $\sigma_{\rm inel}^{h^{14}{\rm N}}$ ratios. The numerators are the ones derived from Eq. (11) using the $\langle n_{\rm wound}\rangle$ values in ANGANTYR and in the fit, respectively, while the denominator is the h^{14}N cross section value provided directly by ANGANTYR. As can be seen, the spread for the 84 data points is not appreciably worse from the fit than for ANGANTYR itself, which means that the fit ought to be a good predictor for other beams and energies.

Similar parametrizations as for ^{14}N above have been done for 14 other common nuclear targets, from ^{2}H to ^{208}Pb, including ^{16}O and ^{40}Ar. (For targets from ^{84}Kr onwards the highest energy point is omitted.) Interpolation is performed for intermediate nuclei.

The $\sigma_{\rm inel}$ end result is illustrated in Fig. 3. The Angantyr values have fluctuations both from Monte Carlo statistics and from the internal geometry algorithms, while the CASCADE curves are based on the fitted $\langle n_{\rm wound}\rangle$, so are smooth from the onset. Nevertheless overall good agreement is found.

The ANGANTYR jump at 20 GeV is caused by two different geometry handlings being used at low and at high energies. At high ones, the full Glauber formalism is used, with fluctuating nucleon sizes. The tuning of free parameters in such an

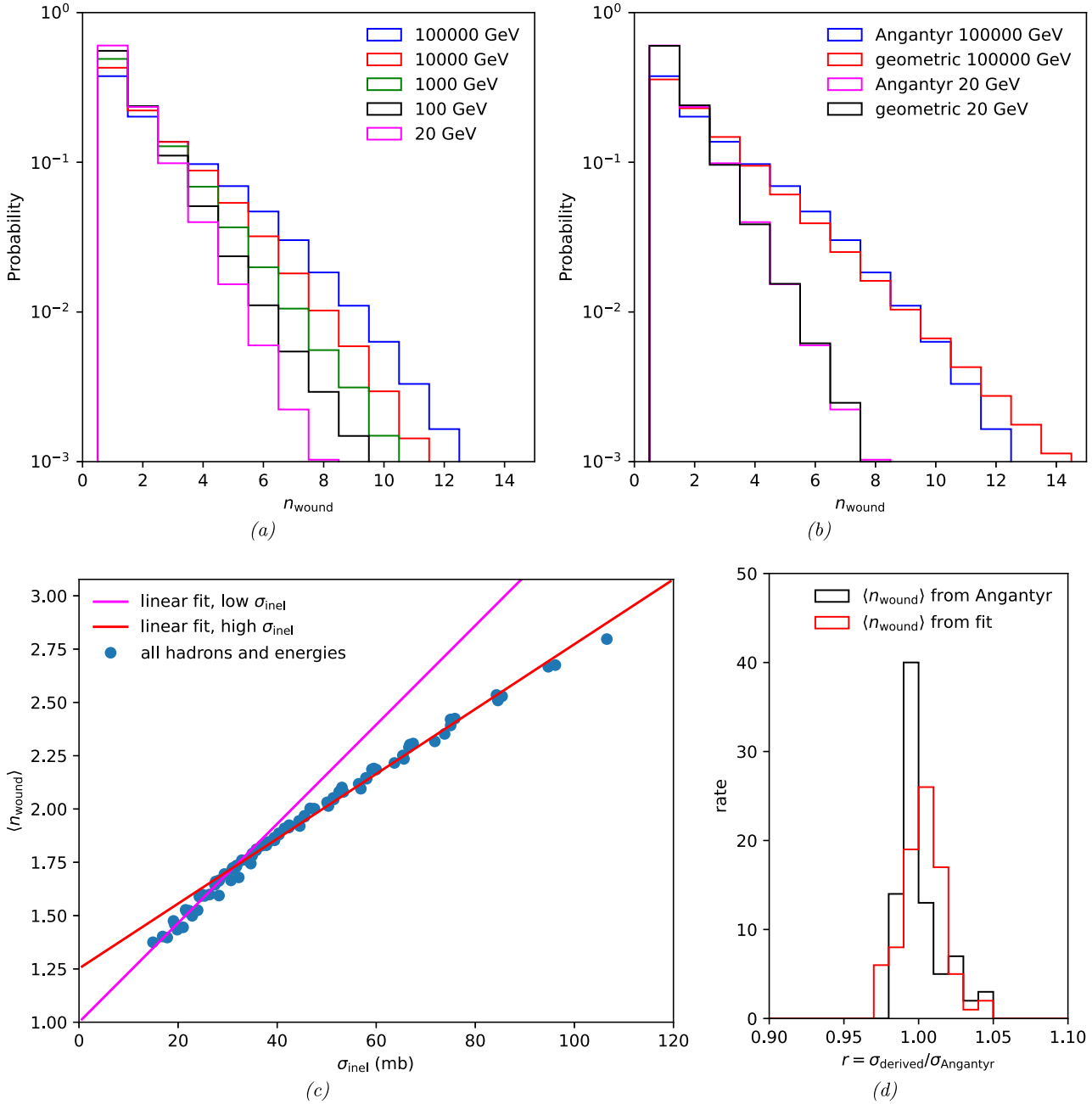

Fig. 2 (**a**) Number n_{wound} of inelastically wounded target nucleons in p^{14}N at a few pN subcollision energies, using full geometry simulation in ANGANTYR. (**b**) Comparison of n_{wound} distribution in ANGANTYR with the simpler geometric series in CASCADE for two energies. (**c**) The $\langle n_{\text{wound}} \rangle$ value for 84 different σ_{inel} ones, as described in the text, and the two resulting linear fit. (**d**) Ratio of derived $\sigma_{\text{inel}}^{hA}$ values to the ANGANTYR ones, for the 84 cases above

approach becomes unstable at low energies, however. Instead a simpler framework is used, where the nucleons have fixed sizes. This gives of the order of 5% higher cross sections below 20 GeV than CASCADE does.

One may note that the detailed event-by-event setup of nuclear geometry, as opposed to the simple geometric series, makes ANGANTYR slower than CASCADE. In the region just above 20 GeV this may give as much as a factor of three slowdown. At higher energies the other generation steps take more time, so proportionately speaking the nuclear geometry becomes less important, even if it does not decrease in absolute terms. To improve the situation, a set of nuclear configurations may be stored and reused, with different incoming beams. Below 20 GeV a simplified geometry handling is used

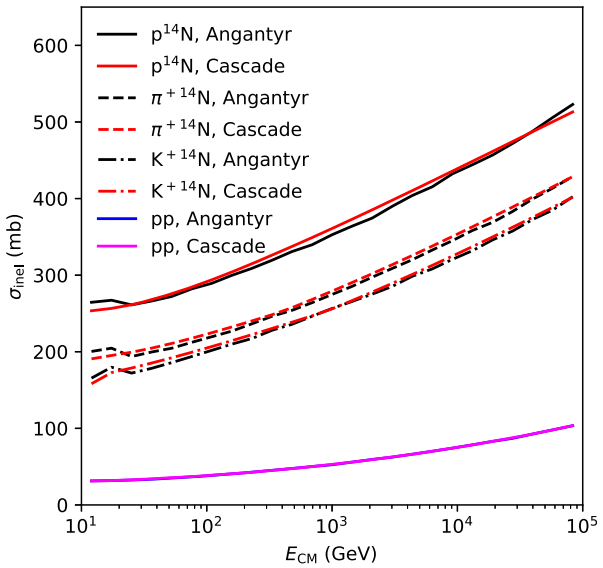

Fig. 3 Energy dependence of the inelastic cross section for some common particles hitting ^{14}N, comparing ANGANTYR and CASCADE. pp collisions are included as a reference

in ANGANTYR, which reduces the ANGANTYR-to-CASCADE discrepancy.

Agreeing inelastic cross sections does not necessarily mean agreeing partial cross sections, not even for the pp starting point. For instance, at 1 TeV the SaS ansatz for inelastic processes is 36.33 mb nondiffractive, two times 5.40 mb single diffractive, and 5.94 for double diffractive, giving a total of 53.07 mb. The ANGANTYR Glauber handling instead gives 36.78 mb, twice 5.63 mb, and 5.01 mb, for a total of 53.04. That is, Glauber gives more single diffraction and less double one in this case.

3.2 Event properties

Event shapes are important for the cascade evolution. In Fig. 4(a) the CM-frame charged-particle rapidity spectrum for inelastic events is compared between p, π^+ and K^+ beams on a p target. The event activity is directly related to the average number of multiparton interactions, which is given by the ratio of the MPI cross section to the inelastic cross section,

$$\langle n_{\mathrm{MPI}} \rangle = \frac{\sigma_{\mathrm{MPI}}}{\sigma_{\mathrm{inel}}}. \tag{12}$$

For the sake of simplicity we here avoid discussing the split between diffractive and nondiffractive topologies [45]. Another potential complication is that the MPI cross section is divergent in the $p_\perp \to 0$ limit, which is addressed by introducing a $p_{\perp 0}$ regularization parameter. Its value need not be the same for all particle combinations, but is for simplicity assumed to be so.

The σ_{MPI} numerator involves the integration of the perturbative parton–parton interaction rate with the parton distributions of the two incoming hadrons. By definition the x-weighted flavour-summed integral is unity for all hadrons, but the shape may differ. One may especially note that the $\pi^+ p$ spectrum peaks at $y < 0$, reflecting differences in the x distributions of π and p. Here it is relevant to recall that only p/n PDFs are well known, with some limited data on $\pi^\pm$ and $K^\pm$, and nothing at all on all the other hadrons.

The σ_{inel} denominator is lower for $\pi^+ p$ than for pp, which translates into a higher multiplicity for the former. $K^+ p$ has an even lower σ_{inel} than $\pi^+ p$, but the $\bar{s}$ quark in the kaon is expected to take a larger fraction of the total momentum than the quarks in the pion, leaving less to low-x gluons, thus giving a reduced σ_{MPI} and $\langle n_{\mathrm{MPI}} \rangle$. The $K^+ p$ process therefore lies below $\pi^+ p$, but still above pp.

Zooming in on the pp curves for a moment, the tiny difference between ANGANTYR and CASCADE comes from a combination of two effects. One is a small divergence in the nondiffractive event generation. The other is the single and double diffractive cross section mix, while the distributions per diffractive event are the same.

The picture is changed when switching to a ^{14}N target, Fig. 4(b). One visible effect is that the distribution maxima are shifted appreciably towards negative rapidities, i.e. in the target direction. This is natural consequence of having 14 nucleons in the target, each with $p_z = -500$ GeV, while there is only one hadron with $p_z = +500$ GeV. So the more nucleons are hit, the more activity in the target direction. Technically the way ANGANTYR and CASCADE achieve this are different, but the outcome similar.

The possibility of having more than one wounded nucleon in h^{14}N collisions also increases the charged multiplicity relative to an hp one. And since $\sigma_{\mathrm{inel}}^{pp} > \sigma_{\mathrm{inel}}^{\pi^+ p} > \sigma_{\mathrm{inel}}^{K^+ p}$ it follows that $\langle n_{\mathrm{wound}}^{p\,^{14}\mathrm{N}} \rangle > \langle n_{\mathrm{wound}}^{\pi^+\,^{14}\mathrm{N}} \rangle > \langle n_{\mathrm{wound}}^{K^+\,^{14}\mathrm{N}} \rangle$. This allows the p^{14}N multiplicity to overtake the $K^+\,^{14}$N one, and close in on the $\pi^+\,^{14}$N one.

The collision energy dependence of the charged multiplicity is shown in Fig. 5(a). For pp ANGANTYR and CASCADE overlap closely – a good sanity check — while the six h^{14}N curves also are clustered. To improve the resolution, Fig. 5(b) shows the h^{14}N curves normalized to the average pp ones. The general trend of an increasing ratio is a natural consequence of an increasing number of subcollisions, which in its turn comes from increasing cross sections. The hierarchy with $\pi^+\,^{14}$N being above and $K^+\,^{14}$N below $p\,^{14}$N is also recognized from Fig. 4(a). Notable is that $\pi^+\,^{14}$N and $K^+\,^{14}$N are closer in CASCADE than in ANGANTYR, which likely is a consequence of the flipping of interacting hadron in the CASCADE nuclear collision chain. Here we thus encounter

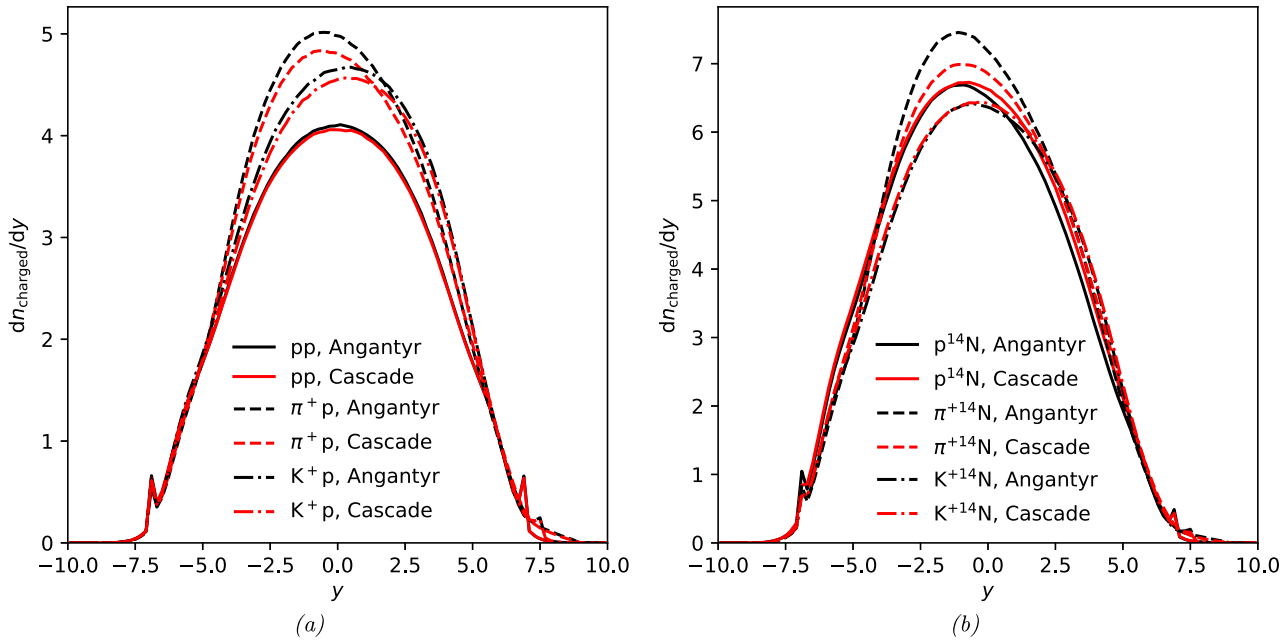

Fig. 4 Rapidity distribution of charged particles, for a 1000 GeV hadron–nucleon CM energy, in the hadron–nucleon rest frame. (**a**) Proton target. (**b**) Nitrogen target

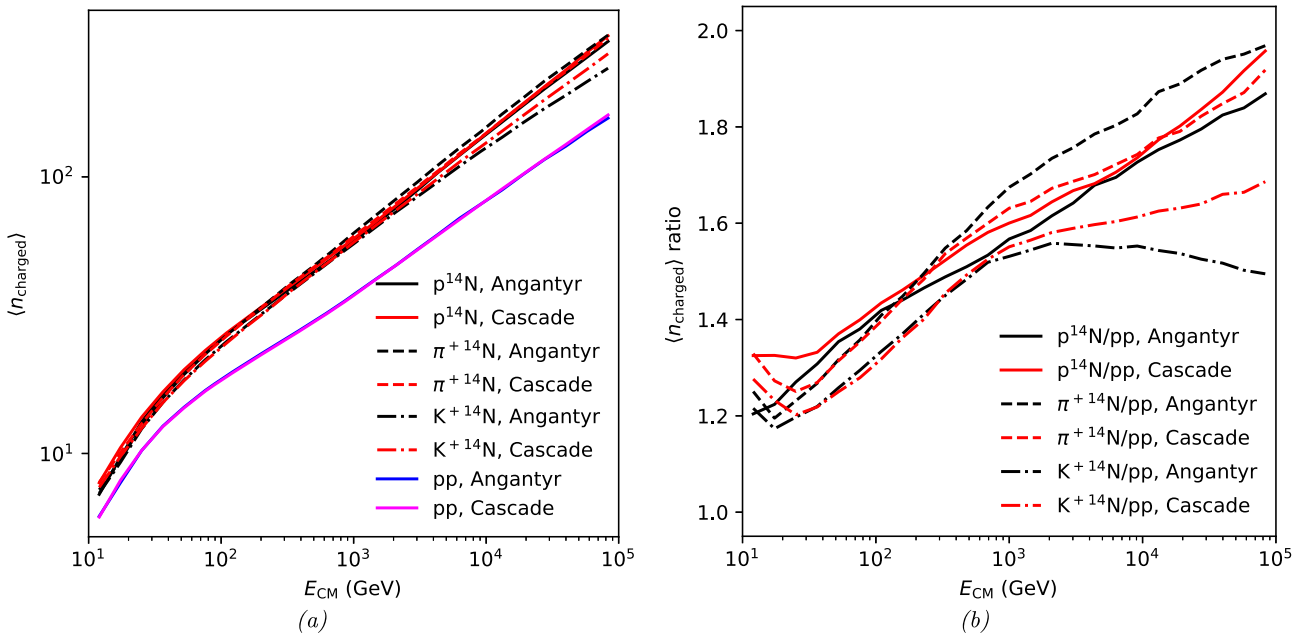

Fig. 5 (**a**) Hadron–nucleon CM energy dependence of the average charged multiplicity for $p/\pi^+/K^+$ beams on a ^{14}N target, comparing ANGANTYR and CASCADE. pp collisions are included as a reference. (**b**) Ratio of the h^{14}N multiplicities to the pp ANGANTYR + CASCADE average one

a clear manifestation of the simplified CASCADE modelling, even if it may be largely masked by the mix of collision processes in an atmospheric cascade. Another weird feature is the larger ratio at the lowest energies, especially for CASCADE, which has no obvious explanation. This is in a transition region, from a simpler longitudinal-string description at low energies to the MPI-based one at higher energies, so the cause may be how this affects secondary collisions. Anyway, on the absolute scale of Fig. 5(a), it does not look so bad.

While the overall charged multiplicity in collisions is relevant, the evolution of an atmospheric cascade is largely driven by the most high-energy hadrons, whether charged or not. Here Fig. 6 shows three interesting features. Firstly, all curves have a peak near $x = 1$, coming from single diffraction, with

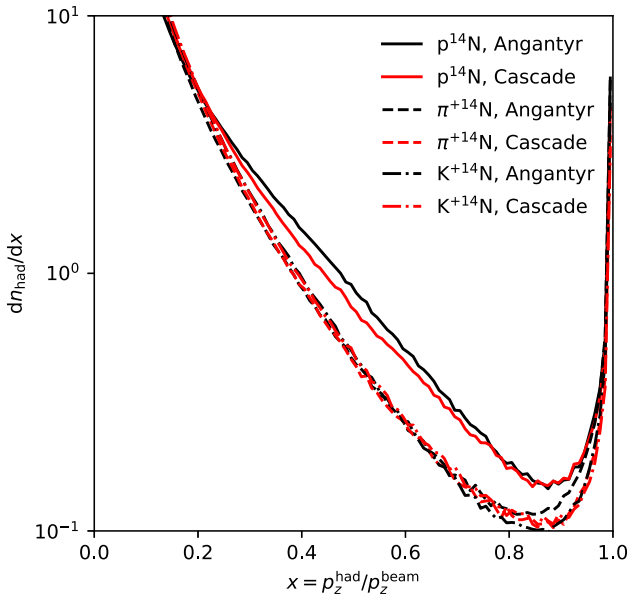

Fig. 6 Longitudinal momentum fraction of stable hadrons for $p/\pi^+/K^+$ beams on an ^{14}N fixed target, for a 1000 GeV hadron–nucleon CM energy, comparing ANGANTYR and CASCADE

the diffracted system in the target region and the beam particle scattering quasi-elastically. Secondly, the proton beam gives more hadrons at intermediate x than the π^+/K^+ ones, which is a direct consequence of the PYTHIA beam remnant handling, where a diquark is allowed to take a larger momentum fraction than a single quark. This is further augmented by a harder fragmentation function into baryons than into mesons, from mass effects. (Potentially also from dynamical mechanisms [40].) And thirdly that ANGANTYR tends to give more medium- and high-x hadrons than CASCADE, even if the differences are not dramatic.

The comparison plots do not go below 10 GeV, but nothing dramatically unexpected happens for lower energies. Cross sections are rather flat, since the decreasing reggeon term and the increasing pomeron one are of comparable magnitude. As a consequence, the number of wounded nucleons in a hA collision would remain fairly flat. But there is a catch, that this number is kinematically restricted by the energy at disposal for inelastic hadron–nucleon subcollisions. This requirement hits harder in the ANGANTYR modelling than in the CASCADE one, and therefore CASCADE generates a somewhat higher multiplicity at low energies. This difference tends to be around or above 10% per collision. Even given the ∼5% higher ANGANTYR inelastic cross section, overall multiplicities are higher in CASCADE. The difference is most notable in the number of low-energy nucleons, and have little impact on higher-energy muons or neutrinos. In the future the modelling in the low-energy region should be contrasted with fixed-target data, and be adjusted as called for.

In passing we note that CASCADE is slower than ANGANTYR in the handling of the lower-energy stages of the cascade, by about 25%, and this is where most of the total time is spent.

3.3 Complete cascades

A simplified model of the atmosphere is used to study the hadronic part of cosmic ray cascades, as a freestanding test of the code prior to inclusion in more sophisticated frameworks. This model is based on the same approach as outlined in [20]. In it, the atmospheric density follows an exponential distribution as a function of the height h above the (sea-level) surface, $\rho(h) = \rho_0 \exp(-h/H)$, where $\rho_0 = 1.225$ kg/m^3 and $H = 10.4$ km. Atmospheric cascades are traced from a 100 km height, neglecting interactions above that. The composition is chosen to be 78.5% nitrogen, 21% oxygen and 0.5% argon, by number density of nuclei. (Often the composition is quoted in terms of number of molecules, and then argon is 1% since it is a noble gas while nitrogen and oxygen form molecules N_2 and O_2.)

There are also some important simplifications. Electromagnetic cascades are not simulated so, once an $e^\pm$ or a photon is produced, nothing more happens to it. Also muon interactions are absent, but muons can decay. The curvature of the earth is neglected, which is only a problem for near-horizon cascades. Bending of charged particles by the earth's magnetic field is also neglected.

Example of properties in such an atmospheric cascade are shown in Fig. 7, for a 10^6 GeV incoming proton. Overall ANGANTYR and CASCADE give similar properties, especially at the beginning of the cascade. At later stages the two diverge, with CASCADE showing a smaller interaction rate with the atmosphere than ANGANTYR. This runs somewhat contrary to CASCADE having a larger particle production rate, even in the early region where interaction rates agree. But we have already noted that low-energy interactions produce approximately 10% more particles in CASCADE than in ANGANTYR. This is visible e.g. in the overall number of hadrons, Fig. 7(b). More particles translates into less energy per particle, which is visible in the rate of hadrons above 10 GeV. Muons are a bit of a special case, since larger production also means more decays, Fig. 7(c). Lower energy also means less time dilation and thus higher probability to decay before reaching the surface, thereby giving a harder spectrum for those that do. The competing effects work out so that muon rates agree well between ANGANTYR and CASCADE, Fig. 7(d), both for all and for higher-energy muons.

Figure 8 shows how the initially hadronic energy leaks over to $e^\pm/\gamma$, to muons, or to neutrinos. The production and decay of π^0 is the main reason why the electromagnetic part soon dominates. The larger early rate of hadrons in CASCADE also translates into a larger early loss of hadronic energy.

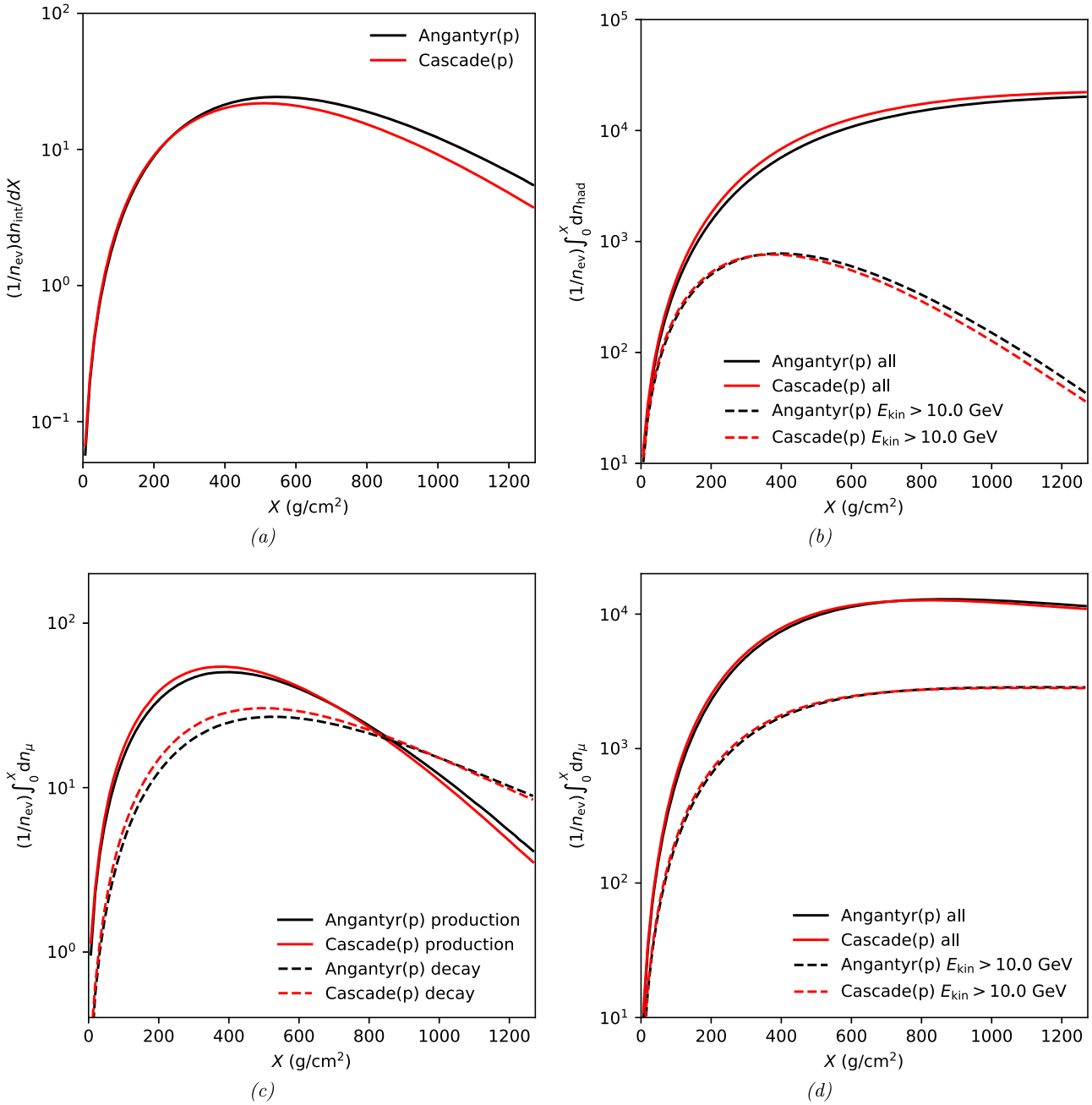

Fig. 7 (**a**) Atmospheric depth X of nuclear interactions. (**b**) Number of hadrons at a depth X, all and those with a kinetic energy above 10 GeV. (**c**) Muon production and decay rates at a depth X. (**d**) Number of muons at a depth X, all and those with a kinetic energy above 10 GeV. Example of properties of a hadronic cascade induced by a vertically incoming proton of 10^6 GeV initial energy, with a lower cutoff of interactions at 0.5 GeV kinetic energy

Later ANGANTYR catches up or even overtakes, but overall differences are tiny.

Obviously results depend on the energy of the cascade initiator. Since most cascades eventually are dominated by low-energy particles, the generated multiplicity grows almost linearly with the initial energy: for the factor 10,000 step between 10^4 and 10^8 GeV the multiplicity increases by almost a factor 5000. A changed energy also affects the balance between collisions and decays. Notably higher-energy $\pi^{\pm}$ and $K^{\pm}$ get increased chances to interact before they decay, owing to time dilation. This leads to a larger fraction of the initial energy going to the electromagnetic component, and lesser to muons and neutrinos, Fig. 8.

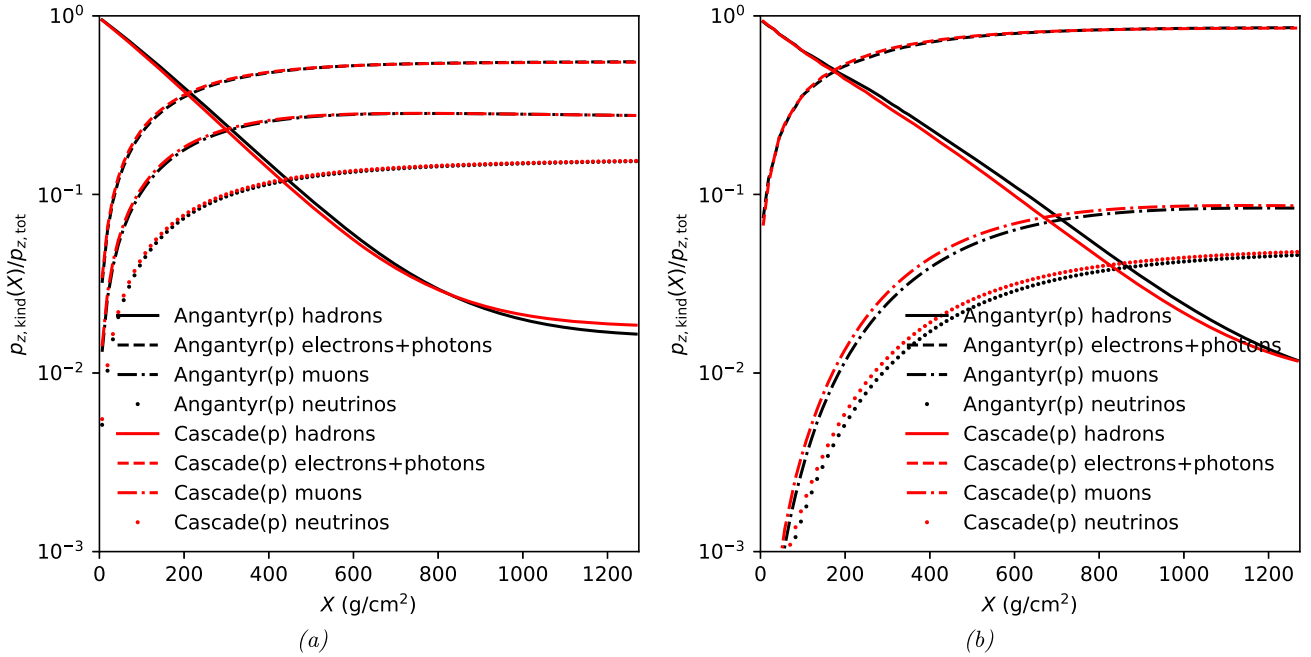

Fig. 8 Fraction of the initial momentum carried by hadrons, by electrons and photons, by muons, and by neutrinos, as a function of X. The initial proton has an energy of (**a**) 10^4 GeV and (**b**) 10^8 GeV, respectively

3.4 Nuclear beams

The area where ANGANTYR excels over CASCADE is that it can handle AA collisions, e.g. from incoming iron nuclei, which usually is chosen as a contrast to the incoming proton case studied so far. There are two specific applications of interest.

Firstly, from the measured energy of the electromagnetic cascade it is possible to estimate the original energy of the incoming projectile. A comparison of the cascade evolution between p and ^{56}Fe projectiles of the same energy allows to understand in what way they differ, and thereby to gain insight on the composition of high-energy cosmic rays. Such a comparison is shown in Fig. 9. The evolution of the iron nucleus cascade starts earlier than that of the p, owing to its larger cross section, and these differences persist. Thus more hadrons, electron/photons, muons and neutrinos are produced in the iron cascade. This decreases the average energy per particle, and as we see this eventually means more hadrons above 10 GeV for the proton cascade. For muons and neutrinos, however, the iron cascade is on top also there. This is related to their larger fraction of the total momentum, mainly at the expense of the electromagnetic cascade part.

Secondly, a standard trick for codes that cannot handle an incoming nucleus is to model it as a superposition of independent nucleon cascades, where the nucleons share the original nuclear energy evenly [21]. This is used e.g. in SIBYLL, and would offer a possibility for CASCADE as well. Figure 10 presents precisely such a comparison where an incident single iron nucleus is compared with 56 separate nucleons, 26 p and 30 n, with a 10^6 GeV energy per nucleon in both cases. As can be seen, the similarity of event properties is striking; event better than one might have guessed. The larger cross section per iron nucleus, times the larger number of wounded nucleons per collision, is expected to compensate fairly well for only being one rather than 56 separate ones, cf. Eqs. (10) and (11). But, in the ANGANTYR model (and by implication also the CASCADE one), wounded nucleons beyond the first one contribute less additional multiplicity than an independent nucleon does. One therefore would expect less particle production in the iron case. Indeed there are some small such effects, notably in the reduced early production of muons, as the nucleus and hadrons retain a somewhat larger fraction of the full energy. But, by the time the cascade comes to the lower atmospheric layers, differences are gone.

One small comment is that ANGANTYR, in each collision, puts all non-wounded nucleons into a new remnant nucleus. This then does not take into account that the remnant is likely to be left in an excited state, from which further nucleons could evaporate. Then ANGANTYR would underestimate the rate at which the original nucleus splits into separate cascades. (There may also be evaporation from the target nucleus but, since the target is at rest, with so low energies that these nucleons will not propagate far.) So, had we noted significant differences above, we could have attributed part of them to the absence of this mechanism. As it happens, we do not even have to use this as a partial explanation of differences.

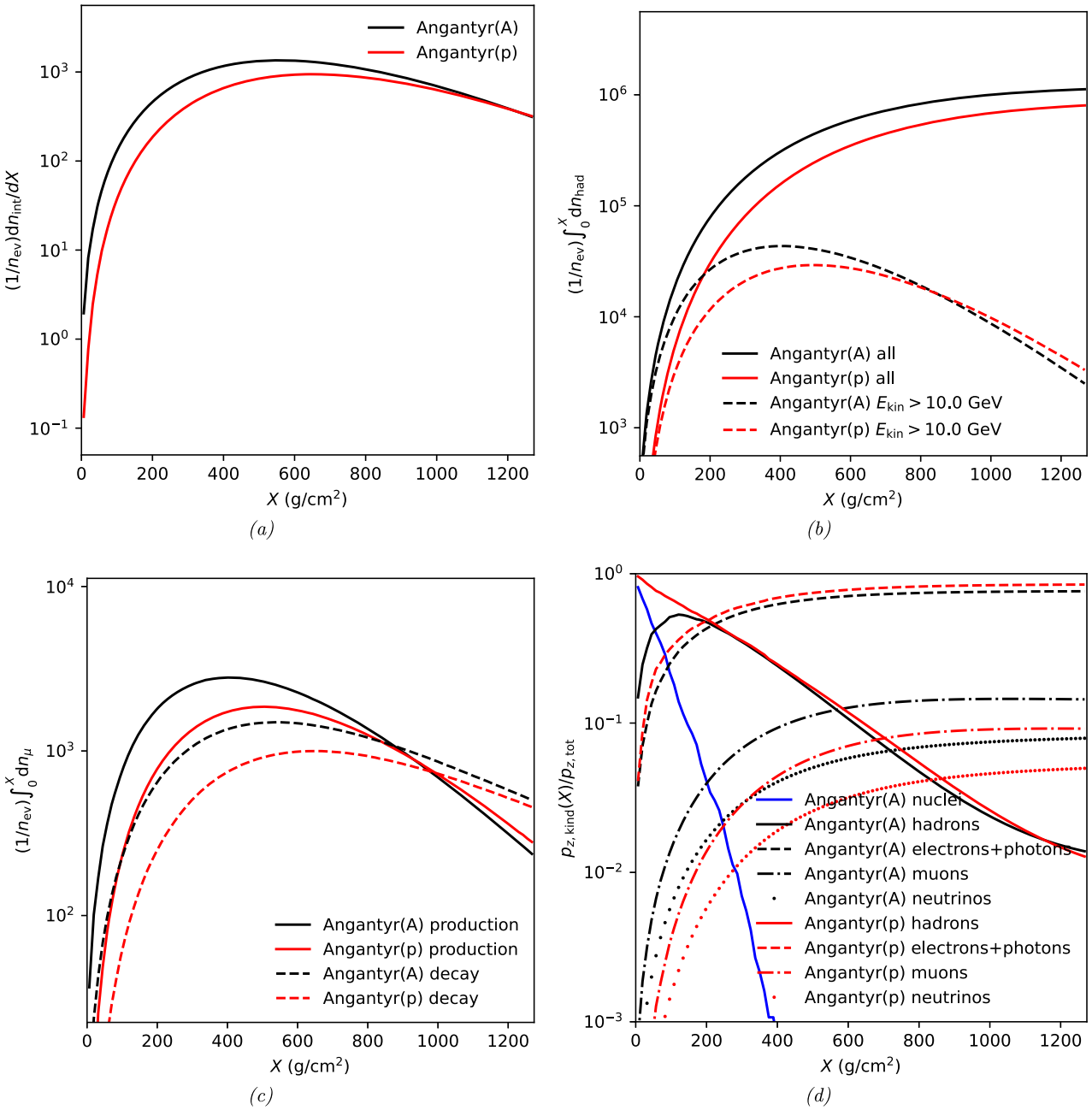

Fig. 9 Example of properties of a hadronic cascade induced by a vertically incoming iron nucleus ("Angantyr(A)") with an energy of 10^6 GeV per nucleon or a single proton ("Angantyr(p)") with an energy of $56 \cdot 10^6$ GeV. (**a**) Atmospheric depth X of nuclear interactions. (**b**) Number of hadrons at a depth X, all and those with a kinetic energy above 10 GeV. (**c**) Muon production and decay rates at a depth X, all and those with a kinetic energy above 10 GeV. (**d**) Fraction of the initial momentum carried by nuclei (only applicable for the iron beam), by hadrons, by electrons and photons, by muons, and by neutrinos, as a function of X

So far the study confirms the standard trick of handling an incoming nucleus as separate nucleons, implying that CASCADE can be used equally well as ANGANTYR for such tasks. There are still differences, however, which were already noted in [21], namely that the distribution in $X_{\max}$ – the position of the maximum of the electromagnetic shower – is wider in the case of a full nucleus, as compared to A individual nucleons. This is expected as taking the average of A individual projectiles naturally will have smaller fluctuations than a single projectile. Since we do not simulate electromagnetic cascades in PYTHIA, we can not easily access $X_{\max}$. Instead we show in Fig. 11 the distribution of the

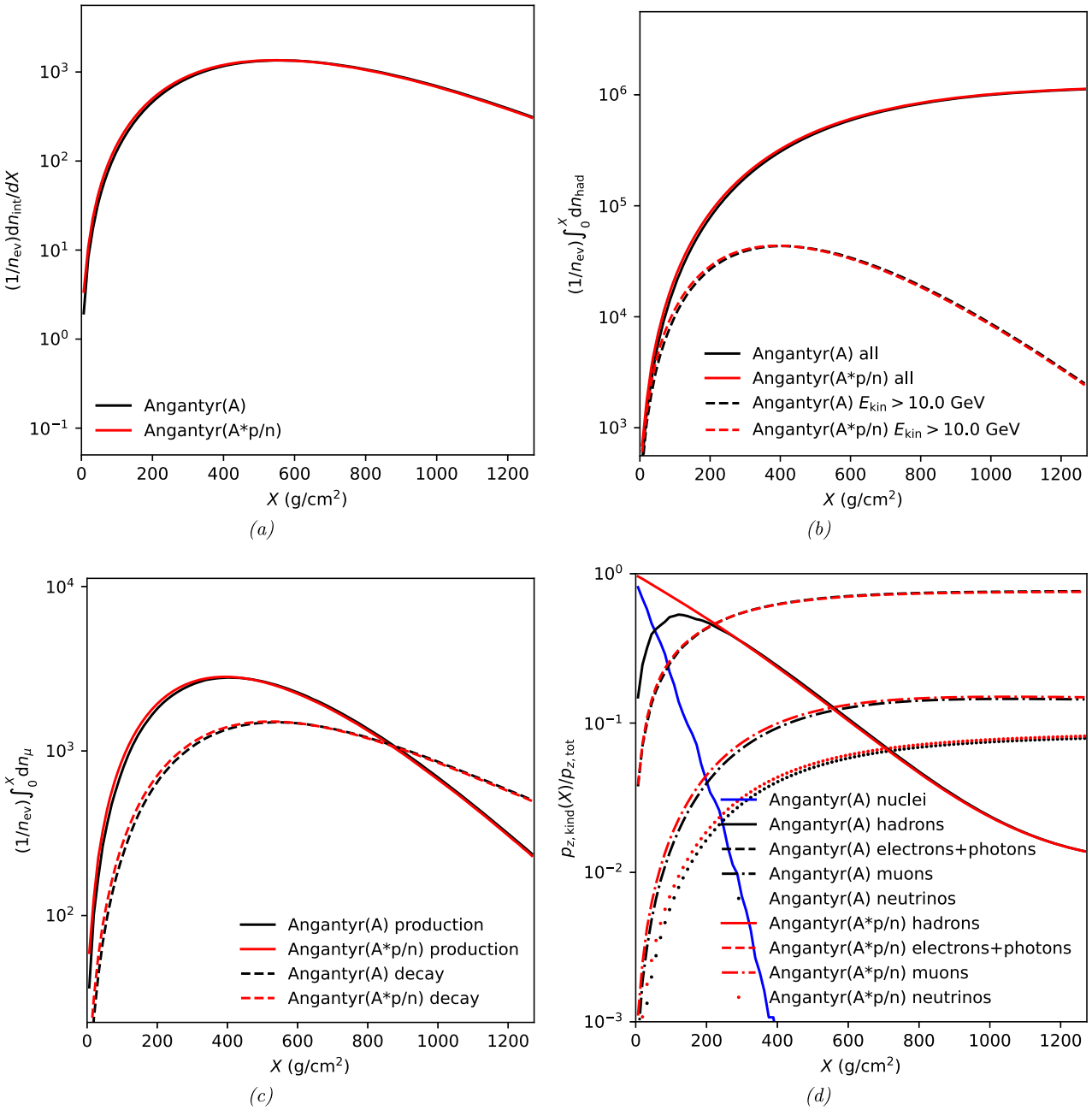

Fig. 10 Example of properties of a hadronic cascade induced by a vertically incoming iron nucleus ("Angantyr(A)") or 56 nucleons ("Angantyr(A*p/n)"), with an energy of 10^6 GeV per nucleon. Frame captions as in Fig. 9

energy-weighted average production depth of electrons and photons in the hadronic cascade, X_{avg}. This should be well correlated with X_{max}, and we find, qualitatively, the same effect. In Fig. 11 we show the effect for two different energies, 56×10^6 GeV and 56×10^4 GeV. It is interesting to note that in both cases the distributions are somewhat wider for the lower energy and also peak a bit earlier. The reason is that pions, which are the main source of electrons and photons, although produced earlier due the increase in cross section at higher energies, also are more time-dilated and more often interact hadronically again, before they have time to decay.

4 Summary and outlook

The main thrust of this article has been to enable variable beams and energies in the ANGANTYR framework of hadron–nucleus and nucleus–nucleus collisions, extending

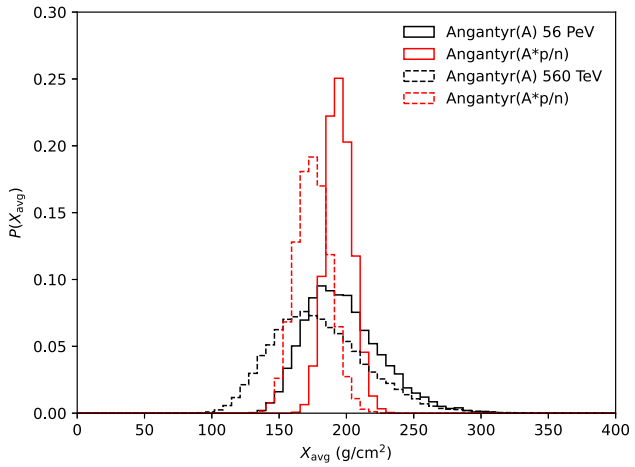

Fig. 11 The distribution of the energy-weighted average production depth of electrons and photons in the hadronic cascade, for a vertically incoming iron nucleus ("Angantyr(A)") compared to 56 nucleons ("Angantyr(A*p/n)") for two different energies, 56×10^6 GeV (solid lines) and 56×10^4 GeV (dashed lines)

on the PYTHIA framework for hadron–hadron ones. This has required significant development of the code, with numerous issues to be solved, mainly administratively, but also in terms of physics modelling. Much of this modelling has been taken over from the code extensions introduced to support CASCADE. That development is now finished, and the code will be made public in an upcoming release of PYTHIA.

Also the CASCADE code has been updated, even if at a more modest scale. CASCADE was originally conceived as a "poor man's" alternative to ANGANTYR, offering the flexibility that ANGANTYR had not. It was anchored to a few key observables of ANGANTYR at fixed energies and beams, notably total and inelastic cross sections, the number of wounded nucleons, and the event activity associated with secondary wounded nucleons. In particular the ANGANTYR bookkeeping of the former has been misleading and required adjustments. Now overall good agreement with the updated ANGANTYR has been restored, at least for higher energies. In this sense CASCADE has served its purpose and could be retired, but its more robust structure makes it a useful backup and cross-check.

A key observation is that ANGANTYR simulation of incoming heavy nuclei, here represented by iron, does not give a cascade evolution that differs significantly from what is obtained if each incoming nucleon is allowed to cascade independently. This implies that CASCADE, designed only to handle a single hadron on a nuclear target, is easily extended also to incoming nuclei.

A small caveat is that we here only considered collisions in air. But PYTHIA is already now used in detector simulation programs like GEANT 4, even if in older incarnations, as mentioned in the introduction. And one of the objectives of the ANGANTYR development work is to make ANGANTYR a valid replacement to those earlier codes, which are in Fortran rather than C++. Sampling calorimeters can here give a quite precise reconstruction of the early shower development, which we have not studied closer in this article, and here the ANGANTYR simulation could have advantages over the CASCADE one. This is a minor point for pp collisions at the LHC, where the primary production of deuterium, tritium and helium is observed to be at very low levels. For AA ones the likelihood of nuclear remnants increases, in particular in the forward direction.

The framework developed here could also have other applications. Incoming neutrinos, from the cosmos or from man-made accelerators, can undergo a charged or neutral current interaction inside the detector, which leads to a subsequent cascade. The primary interaction can then be handled by the basic "old" PYTHIA machinery, and the subsequent evolution by the codes developed here. (With or without the help of GEANT or other tracking codes.) Also, a fraction of high-energy photons interact hadronically with the target material – photoproduction – which leads to new hadronic cascades, where PYTHIA could be used both for a primary and for subsequent interactions.

An important aspect to remember, however, is that neither ANGANTYR nor CASCADE has been tuned to low-energy data. We have noted that this is a region where the two implementations give somewhat different predictions. In the near future it will be relevant to compare with such data, available mainly via RIVET [46], and use these comparisons to improve the modelling. Notably, collider comparisons tend to concentrate on particle production at central rapidities, while here the forward region is more important.

In summary, while the current article represents a big step towards making PYTHIA relevant for a wide variety of particle physics collision processes, we can foresee further developments to further improve the scope and accuracy of the frameworks presented here.

Acknowledgements Work supported in part by the Swedish Research Council, contract numbers 2016-05996 and 2020-04869.

Data Availability Statement This manuscript has no associated data. [Authors' comment: The data generated to produce the results in this article has not been stored, but can be regenerated using example programs distributed with Pythia8 version 317.]

Code Availability Statement Code/software will be made available on reasonable request. [Authors' comment: The code is freely available and is included in Pythia8 (version 317 or later). See https://pythia.org.]

Funded by SCOAP[3].

References

1. A. Aab et al., Nucl. Instrum. Methods A **798**, 172 (2015). https://doi.org/10.1016/j.nima.2015.06.058
2. M.G. Aartsen et al., JINST **12**(03), P03012 (2017). https://doi.org/10.1088/1748-0221/12/03/P03012. [Erratum: JINST **19**, E05001 (2024)]
3. J. Albrecht et al., Astrophys. Space Sci. **367**(3), 27 (2022). https://doi.org/10.1007/s10509-022-04054-5
4. J. Albrecht et al., Road map for the tuning of hadronic interaction models with accelerator-based and astroparticle data (2025). arXiv:2508.21796 [astro-ph]
5. S. Roesler, R. Engel, J. Ranft, in *International Conference on Advanced Monte Carlo for Radiation Physics, Particle Transport Simulation and Applications (MC 2000)*, pp. 1033–1038 (2000). https://doi.org/10.1007/978-3-642-18211-2_166
6. T. Pierog, I. Karpenko, J. Katzy, E. Yatsenko, K. Werner, Phys. Rev. C **92**(3), 034906 (2015). https://doi.org/10.1103/PhysRevC.92.034906
7. T. Pierog, K. Werner, PoS **ICRC2023**, 230 (2023). https://doi.org/10.22323/1.444.0230
8. K. Werner, Phys. Rev. C **109**(1), 014910 (2024). https://doi.org/10.1103/PhysRevC.109.014910
9. S. Ostapchenko, Phys. Rev. D **83**, 014018 (2011). https://doi.org/10.1103/PhysRevD.83.014018
10. S. Ostapchenko, Phys. Rev. D **109**(9), 094019 (2024). https://doi.org/10.1103/PhysRevD.109.094019
11. E.J. Ahn, R. Engel, T.K. Gaisser, P. Lipari, T. Stanev, Phys. Rev. D **80**, 094003 (2009). https://doi.org/10.1103/PhysRevD.80.094003
12. F. Riehn, R. Engel, A. Fedynitch, T.K. Gaisser, T. Stanev, Phys. Rev. D **102**(6), 063002 (2020). https://doi.org/10.1103/PhysRevD.102.063002
13. F. Riehn, R. Engel, A. Fedynitch, PoS **ICRC2023**, 429 (2023). https://doi.org/10.22323/1.444.0429
14. S.A. Bass et al., Prog. Part. Nucl. Phys. **41**, 255 (1998). https://doi.org/10.1016/S0146-6410(98)00058-1
15. M. Bleicher et al., J. Phys. G **25**, 1859 (1999). https://doi.org/10.1088/0954-3899/25/9/308
16. C. Bierlich et al., SciPost Phys. Codeb. **2022**, 8 (2022). https://doi.org/10.21468/SciPostPhysCodeb.8
17. G. Bewick et al., Eur. Phys. J. C **84**(10), 1053 (2024). https://doi.org/10.1140/epjc/s10052-024-13211-9
18. E. Bothmann et al., JHEP **12**, 156 (2024). https://doi.org/10.1007/JHEP12(2024)156
19. C. Bierlich, G. Gustafson, L. Lönnblad, H. Shah, JHEP **10**, 134 (2018). https://doi.org/10.1007/JHEP10(2018)134
20. T. Sjöstrand, M. Utheim, Eur. Phys. J. C **82**(1), 21 (2022). https://doi.org/10.1140/epjc/s10052-021-09953-5
21. J. Engel, T.K. Gaisser, T. Stanev, P. Lipari, Phys. Rev. D **46**, 5013 (1992). https://doi.org/10.1103/PhysRevD.46.5013
22. R. Ulrich, R. Engel, M. Unger, Phys. Rev. D **83**, 054026 (2011). https://doi.org/10.1103/PhysRevD.83.054026
23. J.M. Alameddine et al., PoS **ICRC2023**, 310 (2023). https://doi.org/10.22323/1.444.0310
24. M. Reininghaus, T. Sjöstrand, M. Utheim, EPJ Web Conf. **283**, 05010 (2023). https://doi.org/10.1051/epjconf/202328305010
25. C. Gaudu, M. Reininghaus, F. Riehn, CORSIKA 8 with Pythia 8: Simulating Vertical Proton Showers (2024). arXiv:2412.15094 [astro-ph]
26. S. Agostinelli et al., Nucl. Instrum. Methods A **506**, 250 (2003). https://doi.org/10.1016/S0168-9002(03)01368-8
27. T. Sjöstrand, S. Mrenna, P.Z. Skands, JHEP **05**, 026 (2006). https://doi.org/10.1088/1126-6708/2006/05/026
28. B. Andersson, G. Gustafson, B. Nilsson-Almqvist, Nucl. Phys. B **281**, 289 (1987). https://doi.org/10.1016/0550-3213(87)90257-4
29. B. Nilsson-Almqvist, E. Stenlund, Comput. Phys. Commun. **43**, 387 (1987). https://doi.org/10.1016/0010-4655(87)90056-7
30. C.O. Rasmussen, T. Sjöstrand, Eur. Phys. J. C **78**(6), 461 (2018). https://doi.org/10.1140/epjc/s10052-018-5940-8
31. A. Donnachie, P.V. Landshoff, Phys. Lett. B **296**, 227 (1992). https://doi.org/10.1016/0370-2693(92)90832-O
32. G.A. Schuler, T. Sjöstrand, Phys. Rev. D **49**, 2257 (1994). https://doi.org/10.1103/PhysRevD.49.2257
33. G.A. Schuler, T. Sjöstrand, Z. Phys. C **73**, 677 (1997). https://doi.org/10.1007/s002880050359
34. E.M. Levin, L.L. Frankfurt, JETP Lett. **2**, 65 (1965)
35. H.J. Lipkin, Phys. Rep. **8**, 173 (1973). https://doi.org/10.1016/0370-1573(73)90002-1
36. T. Sjöstrand, M. Utheim, Eur. Phys. J. C **80**(10), 907 (2020). https://doi.org/10.1140/epjc/s10052-020-8399-3
37. M. Glück, E. Reya, I. Schienbein, Eur. Phys. J. C **10**, 313 (1999). https://doi.org/10.1007/s100529900124
38. M. Botje, Comput. Phys. Commun. **182**, 490 (2011). https://doi.org/10.1016/j.cpc.2010.10.020
39. G. Ingelman, P.E. Schlein, Phys. Lett. B **152**, 256 (1985). https://doi.org/10.1016/0370-2693(85)91181-5
40. M. Fieg, F. Kling, H. Schulz, T. Sjöstrand, Phys. Rev. D **109**(1), 016010 (2024). https://doi.org/10.1103/PhysRevD.109.016010
41. V.N. Gribov, Sov. Phys. JETP **29**, 483 (1969)
42. W. Broniowski, M. Rybczynski, P. Bozek, Comput. Phys. Commun. **180**, 69 (2009). https://doi.org/10.1016/j.cpc.2008.07.016
43. M. Rybczynski, G. Stefanek, W. Broniowski, P. Bozek, Comput. Phys. Commun. **185**, 1759 (2014). https://doi.org/10.1016/j.cpc.2014.02.016
44. C. Rosenkvist, Non-diffractive nuclear excitations in Angantyr. Master's thesis, Lund University. Student Paper (2023). https://lup.lub.lu.se/student-papers/search/publication/9131895
45. C.O. Rasmussen, T. Sjöstrand, JHEP **02**, 142 (2016). https://doi.org/10.1007/JHEP02(2016)142
46. C. Bierlich, A. Buckley, J.M. Butterworth, C. Gutschow, L. Lonnblad, T. Procter, P. Richardson, Y. Yeh, SciPost Phys. Codeb. **36**, 1 (2024). https://doi.org/10.21468/SciPostPhysCodeb.36